Renewable Energy 194 (2022) 788–804

Contents lists available at ScienceDirect

Renewable Energy

journal homepage: www.elsevier.com/locate/renene

Laboratory and numerical study on innovative grouting materials applicable to borehole heat exchangers (BHE) and borehole thermal energy storage (BTES) systems

Hossein Javadi [a, *], Javier F. Urchueguía [a], Borja Badenes [a], Miguel Á. Mateo [a], Ali Nejad Ghafar [b], Ojas Arun Chaudhari [c], Giedrius Zirgulis [c], Lenin G. Lemus [a]

[a] Information and Communication Technologies versus Climate Change (ICTvsCC), Institute of Information and Communication Technologies (ITACA), Universitat Politècnica de València (UPV), Camino de Vera S/N, 46022, Valencia, Spain
[b] Implenia Sverige AB, Liljeholmsstranden 5, 117 43, Stockholm, Sweden
[c] RISE Research Institutes of Sweden, Department Instrastructure and Concrete Construction, Drottning Kristinas väg 26, 114 28, Stockholm, Sweden

ARTICLE INFO

Article history:
Received 27 September 2021
Received in revised form
16 April 2022
Accepted 29 May 2022
Available online 1 June 2022

Keywords:
Shallow geothermal energy
Borehole heat exchanger
Borehole thermal energy storage
Enhanced grout
Phase change material
Thermal conductivity

ABSTRACT

In this study, a laboratory-scale prototype of a borehole field has been designed and built to assess various innovative grouting products in a fully controlled environment. Three novel grout formulations are developed and evaluated: enhanced grout, a mixture of enhanced grout and microencapsulated phase change material, and a mixture of enhanced grout and shape stabilized phase change material. The objective is to evaluate the enhancement in their thermal properties (i.e., thermal conductivity and thermal energy storage capacity) compared to those using a commercial reference grout. Besides, three-dimensional numerical modeling is performed to provide a better understanding of the heat transfer and phase transition inside and outside the grout columns and to study the capability of the developed grouts to be used in a borehole heat exchanger or as borehole thermal energy storage system. To the best of the authors' knowledge, there have been just a few numerical studies on using phase change materials inside borehole heat exchangers to assess thermal energy storage applications. The experimental and numerical results showed much higher efficiency of the grout developed with a high thermal conductivity than the reference grout in terms of heat transfer in both the grout column and the surrounding sand. Furthermore, the results indicated the noticeable influence of the microencapsulated phase change material's presence in the grout formulation in terms of heat absorption/storage during the phase transition (from solid to liquid). However, it is concluded that reengineering shape stabilized phase change material should be conducted to make it more appropriate for thermal energy storage applications.

1. Introduction

Shallow geothermal energy (SGE) is becoming a key driver in the energy transition to a future without fossil fuels and promoting renewable energies. SGE can play a vital role in the reduction of CO_2 emissions from the building air-conditioning sector. The ground source heat pump (GSHP) falls into the SGE division, in which a borehole heat exchanger (BHE) is considered one of the main components [1–5]. The most widely developed underground thermal energy storage (UTES) systems are based on boreholes (borehole thermal energy storage (BTES)) or aquifers (aquifer thermal energy storage (ATES)) and are mainly applied for seasonal energy storage. Energy storage by ATES systems requires a suitable aquifer, where at least two thermal wells are installed. ATES systems extract groundwater from a well, exploit it energetically, and then re-inject it into the aquifer through another well. Furthermore, thermal energy can be stored underground employing BTES systems. BTES systems use the underground for storing thermal energy and are adaptable to almost any ground conditions. These systems consist of one or several boreholes to store energy underground for later use, in general seasonally, with several typologies, from single buildings to large-scale commercial buildings or district heating network systems coupled to a GSHP. BTES allows heat to be injected into the ground during the summer and

Abbreviations: L, Liter.

* Corresponding author.
E-mail address: hjavadi@upv.es (H. Javadi).

https://doi.org/10.1016/j.renene.2022.05.152

Nomenclature

C_{mush}	Mushy zone constant
C_p	Specific heat capacity ($J \cdot kg^{-1}\ K^{-1}$)
g_i	Gravitational acceleration ($m \cdot s^{-2}$)
h_t	Total enthalpy ($J \cdot kg^{-1}$)
h_{sens}	Sensible heat enthalpy ($J \cdot kg^{-1}$)
h_{lat}	Latent heat enthalpy ($J \cdot kg^{-1}$)
h_{ref}	Reference enthalpy ($J \cdot kg^{-1}$)
L_f	Latent heat of phase change material ($J \cdot kg^{-1}$)
S_e	Source term of energy equation
S_i	Source term of momentum equation
t	Time (s)
T	Temperature (K)
v_i	velocity component of the i direction ($m \cdot s^{-1}$)
v	Circulation fluid velocity ($m \cdot s^{-1}$)
$\vec{V}$	Velocity vector ($m \cdot s^{-1}$)
v_p	Velocity of solidified material moving throughout the computational cells ($m \cdot s^{-1}$)

Greek Symbols

β	Liquid fraction of phase change material
μ	Dynamic viscosity (Pa·s)
ρ	Density ($kg \cdot m^{-3}$)
λ	Thermal conductivity ($W \cdot m^{-1}\ K^{-1}$)

Abbreviation

BHE	Borehole heat exchanger
BTES	Borehole thermal energy storage
GHE	Ground heat exchanger
GSHP	Ground source heat pump
MPCM	Microencapsulated phase change material
SSPCM	Shape stabilized phase change material
SGE	Shallow geothermal energy

extracted to satisfy the heating needs in the winter or vice versa [6,7].

To improve such systems and make them more cost-competitive for consumers, materials that enhance thermal storage in BHEs are currently being studied. Numerical analyses have been conducted to verify the impact of the use of phase change materials (PCMs) in geothermal borehole grouting, e. g. using a mixture of n-decanoic acid and lauric acid (DLC) [8], and found that the use of PCM has certain advantages over the use of standard grouting [9,10]. Thermal energy partial storage and release from changes in the PCM structure reduce the sensible heat exchange in the soil [11]. The use of microencapsulated PCM (MPCM) could decrease the required BHE length (about 7%) when the thermal conductivities of the PCM and grout are close to each other for a given PCM melt temperature [12]. The use of PCM grouts with a thermal conductivity comparable to an ordinary grout has been observed to improve the efficiency and operational stability of a GSHP system [13,14], validated by experimental results [15]. Enhanced thermal performance is observed with the addition of PCM to the grout in different borehole configurations: coaxial ground heat exchangers (GHEs) [16], U-tube GHEs [17–19], horizontal GHEs [20–22], experimental GHEs [23–25], novel vertical air-soil heat exchangers (VASHEs) [26] or earth-to-air heat exchangers (EAHEs) ventilation systems [27]. The performance analysis of cascade PCM heat exchangers in geothermal district heating systems has also been carried out [28].

The use of thermal storage enhancers in BTES has also been generally analyzed, noting that the performance of the energy storage system can be significantly improved by incorporating PCM storage units [29] and its effect on the electric load shifting in building demand-side management [30]. The effect of the energy capacity of PCM during the charge–discharge phases with latent heat storage has also been analyzed [31,32], but the high-frequency intermittent mode might not be suitable for BHE with PCM backfilling [33]. Some examples of numerical modeling and energy simulations of GHEs are BHEs integrated with hydrated sodium sulfate as thermal energy storage (TES) [34], PCM-Sand mixture ring around the borehole wall of a BHE [35], PCM containers implemented in building foundation piles as a BHE [36,37]. Additionally, family residences using a GSHP system integrated with a PCM storage tank [38], MPCM slurry as the working fluid in a tree-shaped BHE [39], and partially charging and discharging a PCM TES tank in a commercial building [40]. Also, two examples of PCM usage in the horizontal GHE include horizontal GHE integrated with the panel form of PCM as TES [41] and horizontal GHE integrated with microencapsulated paraffin and soil as TES [42]. Also, two kinds of PCMs have been evaluated for latent heat thermal energy storage (LHTES) applications [43].

Nevertheless, considering the past articles being studied, there have been only a few numerical studies on implementing PCM in the BHEs, and the TES application of BHEs has not yet been explicitly examined. Therefore, in this research, two laboratory tests, including single-column and four-column tests, have been conducted to evaluate various grouting materials that can be used in the BHE or BTES systems. In the first test, a single grout column containing a reference grout (commercial grout) is examined to learn more about the system's behavior, the potential defects, solutions, and verification of the numerical modeling. In the second test, four grout columns backfilled with different materials such as reference grout, enhanced grout, enhanced grout with MPCM, and enhanced grout with shape stabilized PCM (SSPCM) were simultaneously tested to provide the same conditions for all grout columns. Moreover, 3D numerical simulation of the two laboratory tests is conducted to understand better the heat transfer and phase transition occurrence inside the sandbox.

2. Laboratory test

The laboratory test was principally based on the circulation of a heat carrier fluid with the constant temperature inside a pipe centrally located in a sandbox's grout column. The grout thermal conductivity variation used in the grout column are reflected in different temperature field changes inside and outside the column, which were measured using different sets of thermocouples. Each grout column was placed in the sand which was compacted using water and then completely drained out to simulate soil conditions like a BHE/BTES system. The sand was chosen due to simplicity in handling (the box was filled and unloaded using shovels) and economic reasons [44,45]. Also, the compaction with water procedure assumingly created the same soil density, water saturation, and thermal properties around columns. Thermo-physical properties were measured once based on the same assumption. The grout columns used in the experiments are 190 mm in diameter and 1000 mm in height. A single Polyethylene (PE) pipe with 20 mm in diameter was located in the center of each column for heat injection through water circulation. Although the test setup is larger than bench laboratory tests, the grout columns' heights are still small compared to the real borehole. This test did not reflect reality fully; instead, it created controlled conditions focused on grout

thermal performance and temperature distribution around the heat source (pipe). The single pipe was chosen for the sake of simplicity as a heat injector. The circulation fluid temperature was varied between 20 °C and 50 °C to trigger the temperature field change. The temperature range was chosen on the basis of the PCMs' melting and crystallization temperatures (sufficiently high and low than the phase transition temperatures), which was planned to be used in the laboratory test.

2.1. Description of the laboratory test

In this study, the sandbox was used in the test rig was built on two wooden pallets to provide a flat and firm basis for safe transportation (Fig. 1 (a)). The sandbox walls were made of 12 mm laminated water-resistant plywood sheets, which are widely used to prepare concrete molds in the building industry. The supporting frames were made of 100 × 50 mm wood boards to prevent any potential deflection in the walls. The sandbox was then completely insulated (from all sides) with 100 mm styrofoam thermal panels (see Fig. 1 (a)). A circulation pump was used to circulate the heat carrier fluid (i.e., water) within the system. An open surface water tank (60-L plastic container) with a heater was employed in the test setup to provide the designated constant temperature in circulating water along with the experiments. The temperature of water in the heating phase (heat from 20 °C to 50 °C and maintain a constant level) was controlled by a digital thermostat and a 2 kW heater. To provide the possibility of heating and cooling for the circulating water (without changing the test setup), the water tank, with the installed heating system, was placed in a cooling chamber. To allow cool-down in the cooling phase, as shown in Fig. 1 (b), (reduce the water temperature from 50 °C to 20 °C and maintain in constant level), the water tank was placed in a cooling chamber with a temperature set to 0 °C (work in continuous mode). The water tank's heating system (including a heater, a digital thermostat, and a temperature sensor) was kept operational during the cooling phase to prevent water from overcooling. Moreover, the molds used for casting the grout columns are cardboard molds, which could be used for casting concrete foundations. The cardboard molds' inner walls were covered with plastic tape to prevent moisture loss from the fresh grout mix (Fig. 2 (a)). The PE pipe was placed in the mold's center and secured with two metal lids (Fig. 2 (b)). Besides, a metal bar was placed inside the pipe during the setting time to support the PE pipe and keep it straight while the grout was still in fluid form.

2.2. Mixing, casting, and curing of the developed grouting materials

A twin shaft handheld mixer was used in this study to obtain a proper dispersion of the solid particles in the grout suspension during the mixing process. A mixer with a maximum rotation speed of 950 rpm was applied in all mixing processes. The dual propellers rotating in opposite directions apply sufficient shear to provide the required dispersion. The mixing procedure was kept the same for all five grout columns (single- and four-column tests) as follows:

- The dry component was poured in a plastic container and premixed in dry conditions with the same mixer (with low speed).
- The required water (the amount of water needed for one gout column) was poured into another plastic container.
- The dry mixed components were slowly added to the water while mixing at a low speed for about 2 min.
- The primary mixing was then continued for about four more minutes, resulting in 6 min of the mixing process in total.

The casting process of each grout column was performed manually by filling the mold (Fig. 3 (a)) through a funnel with an attached hose. The end of the hose reached the bottom of the mold to provide the possibility of bottom-up filling. After demolding, the grout columns were wrapped in plastics and filled with water for curing for up to 28 days (Fig. 3 (b)). Two grout formulations were used to prepare the grout columns in this research, with and without PCM. All the quality control tests were performed on fresh grout, e.g., wet density test, marsh cone test, the flow table test, and bleeding test. Furthermore, quality control tests were also conducted for the hardened grout, including a compressive strength test, thermal conductivity test, and latent heat test (only on the grout with PCM).

Fig. 1. The single-column test rig: (a) The sandbox, cooling chamber, and data acquisition system, and (b) Water tank with a mounted heating system inside the cooling chamber.

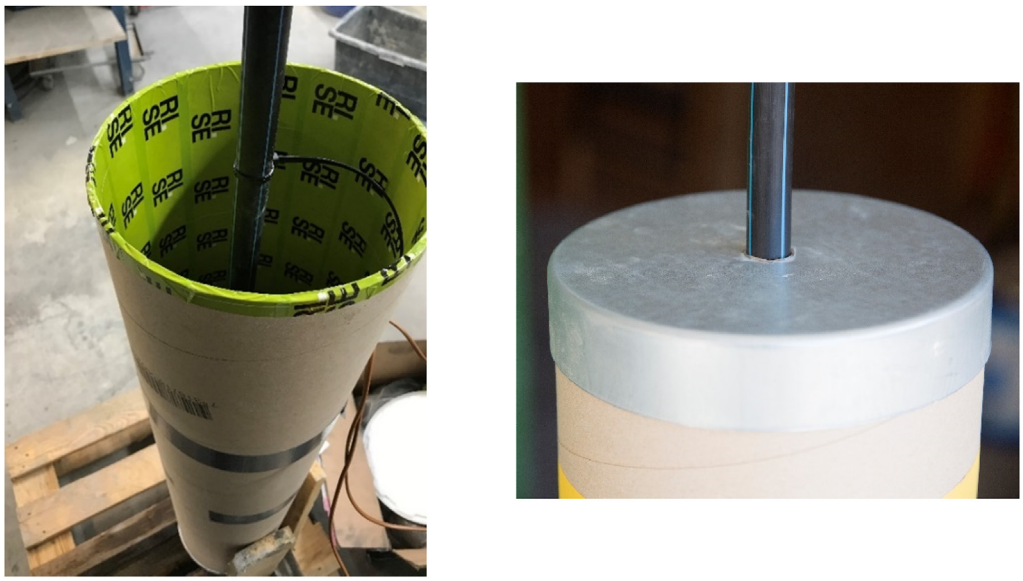

Fig. 2. Grout column used in the tests: (a) Cardboard mold fixed on a wooden pallet and the inner mold surface covered by plastic tape, and (b) Metal lid used to center the PE pipe.

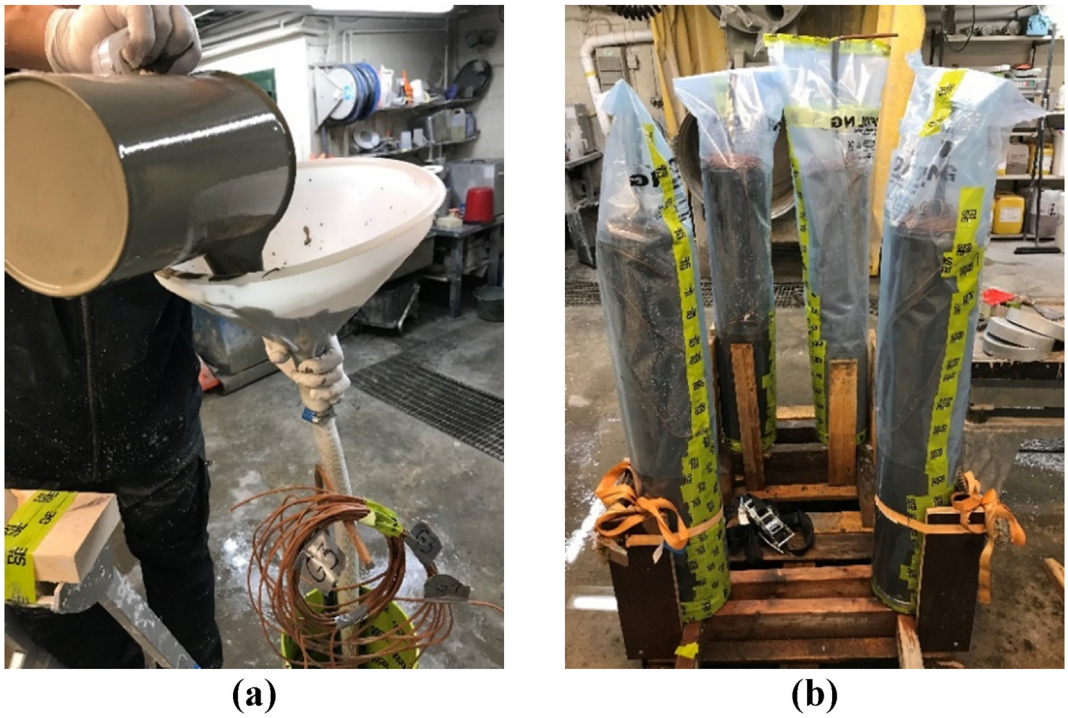

Fig. 3. Casting and curing of the grout columns: (a) Filling the grout through the funnel, and (b) Curing the grout columns.

2.3. Single-column test

2D schematics, the geometrical parameters, and a picture of the sandbox in the single-column test are shown in Fig. 4. The sandbox was a thermally insulated cubic box with a 1000 mm edge length, comprising one column with 190 mm in diameter placed in the center of the box. The column consisted of circulation fluid, single pipe, reference grout, and silica sand, which was previously fully saturated with water to provide sufficient compaction and then drained out. The circulation fluid entered at the top of the PE pipe with 1000 mm length and exited from the bottom. In this test, a flow rate of 1800 L/h was considered for the circulating fluid to assure turbulent flow conditions. Thermo-physical properties of the sandbox and geometry details, simulation conditions, and thermocouple positions for the first test are presented in Tables 1 and 2, respectively.

In the test setup, the temperature field in the sandbox (inside and around the grout column) was measured using several

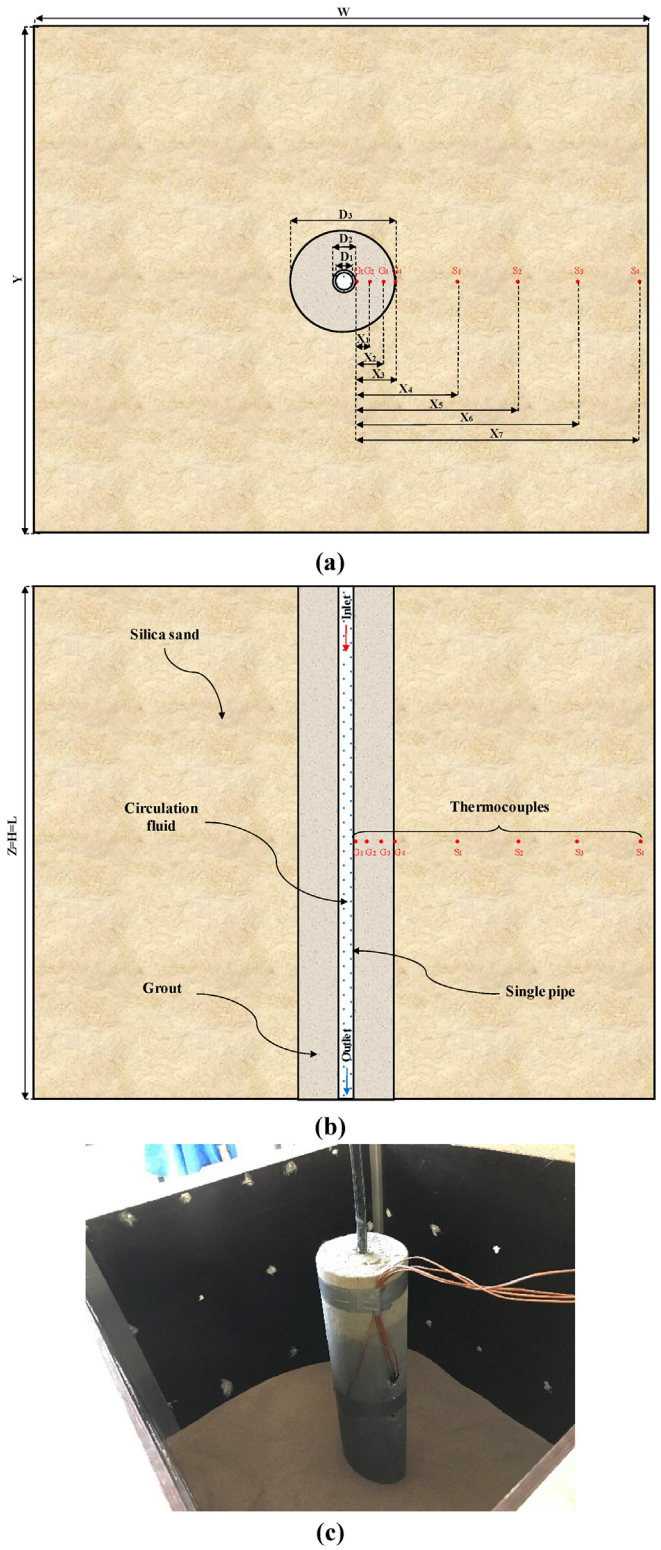

Fig. 4. 2D schematics, the geometrical parameters, and the picture of the sandbox in the single-column test: (a) Top view, (b) Front view, and (c) The grout column installed in the box filled with silica sand.

thermocouples located at various distances from the center of the grout column (Fig. 4 (a), and (b)). As illustrated in the figures, in the single-column test, eight temperature sensors (G_1, G_2, G_3, G_4, S_1, S_2, S_3, and S_4) were installed inside the sandbox to measure the temperature at various distances at a depth of 500 mm. The first thermocouple was attached to the surface of the centrally located pipe. The thermocouples in each grout column were secured in position along with a wooden stick using cable ties so that the heat transfer in the grout column was not significantly affected (Fig. 5).

2.4. Four-column test

In the four-column test, the test setup is slightly modified to perform the test with the four grout columns simultaneously as described below:

1. Grout column 1 made of a commercially available grout as a reference
2. Grout column 2 made of grout with high thermal conductivity
3. Grout column 3 made of grout with high thermal conductivity and high thermal storage capacity by incorporation of MPCM
4. Grout column 4 made of grout with high thermal conductivity and high thermal storage capacity by incorporation of SSPCM

Fig. 6 depicts 2D schematics and the geometrical parameters of the sandbox in the four-column test. The sandbox was divided into four sections using 40 mm extruded polystyrene insulation plates to accommodate all four grout columns in the set. Accordingly, two of the four thermocouples installed in the sand around the grout column in the single-column test must be discarded, applying two thermocouples with smaller distances. Therefore, as shown in Fig. 6 (a) and (b), six temperature sensors of G_1, G_2, G_3, G_4, S_1, and S_2 were installed inside each section of the sandbox to obtain the temperature data at various distances at a fixed depth of 500 mm. Thermo-physical properties of the sandbox and geometry details, simulation conditions, and thermocouple positions for the second test are given in Tables 1 and 2, respectively. Note that there was a relative error of up to 10% in the thermo-physical properties of the developed grouting materials measured in the laboratory. In this setup, similar PE pipes (with the same diameter) were applied in four grout columns as used in the previous test. The flow rate of 1800 L/h is calculated based on circulation pump technical data and divided between four pipes/columns; nevertheless, the fluid flow regime is still turbulent in all four columns. To reduce the possibility of moisture loss in the sand (and consequently the possibility of change in the sand thermal conductivity in time during the test), the inner walls of the test box were covered with plastic. As in the previous test, the box was filled with silica sand after installing the grout columns. Afterward, the sand was compacted using water and then completely drained out (Fig. 7 (a)). The centrally located PE pipes in the grout columns were symmetrically connected with the brass fittings to connect the grout columns to the circulation pump, ensuring similar flow rates in all four grout columns (Fig. 7 (b)). Also, all pipes and hoses were thermally insulated.

3. Numerical simulation

In the numerical approach, a 3D unsteady numerical model of the sandbox is simulated by using Ansys Fluent 18 software. The most common commercially available CFD programs technique is the finite volume method (FVM) applied in this numerical modeling. FVM is efficient in conserving the continuity, momentum, and energy equations, even in coarse grids. Besides, FVM benefits memory usage and speed in turbulent flow computation, higher speed flows, vast geometries, etc. Since the sandbox was thermally insulated in both tests, including the single-column and four-column tests, the insulation walls (outer walls) were considered adiabatic in the numerical simulation. Additionally, in the four-column test, where the sandbox was divided into four sections

Table 1
Thermo-physical properties of the sandbox.

Material		Thermal conductivity (W/m.K)	Density (kg/m^3)	Specific heat capacity (J/kg.K)	Latent heat (kJ/kg)	Phase transition temperature (°C)
Circulation fluid (Pure water)		0.6	998	4260	–	–
Pipe (Standard PE 100)		0.421	960	2600	–	–
Grout	Reference grout	2	1520	750	–	–
	Enhanced grout	2.7	2000	800	–	–
	Enhanced grout + MPCM	1.025	1510.00	1593.15	24.36	23.5–28.8
	Enhanced grout + SSPCM	2.17	1760.00	1959.12	25.00	20–30
Silica sand		2.65	2647	830	–	–

Table 2
Geometry details, simulation conditions, and thermocouple positions.

Parameters					Value		Unit
Sandbox, W × Y × Z					1000 × 1000 × 1000		mm^3
Pipe length, L					1000		mm
Pipe inner diameter, D_1					16		mm
Pipe outer diameter, D_2					20		mm
Grout column diameter, D_3					190		mm
Grout column depth, H					1000		mm
Insulation wall thickness, I_1					40		mm
The initial temperature of the circulation fluid					20		°C
Flow rate					1800		liter/h
Thermocouples distance from the surface of the pipe (G_1 at the surface)	X_1	28	X_8	28			mm
	X_2	56	X_9	56			mm
	X_3	86	X_{10}	84			mm
	X_4	185	X_{11}	159			mm
	X_5	285	X_{12}	234			mm
	X_6	385					mm
	X_7	485					mm
Thermocouples distance from the bottom of the sandbox, I_2					500		mm

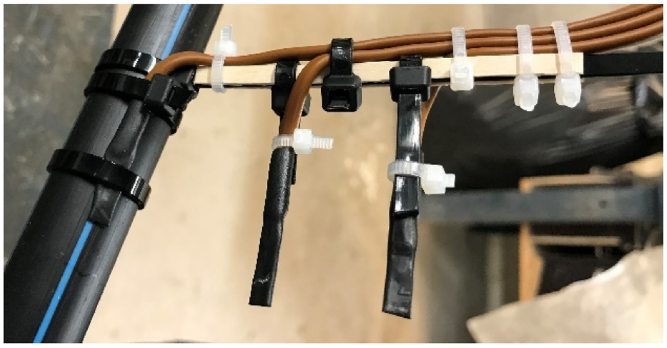

Fig. 5. Thermocouples with waterproof covers and a wiring system were fixed in position along with a wooden stick.

by the insulation plates, these walls were also selected as adiabatic walls. Moreover, the contact thermal resistance of different interfaces is insignificant, and all joints of the components were considered temperature-coupled walls when modeling the tests numerically. A velocity-inlet condition with a constant velocity and variable temperature is set for the inlet boundary, and a pressure-outlet condition is chosen for the outlet boundary. The circulation fluid flow inside the pipe is incompressible and forced. The circulation fluid and sand are assumed to be temperature independent, isotropic, and homogeneous. Given that the Reynolds number of the fluid circulating inside the pipe for both tests is in the turbulent regime range, a standard k-epsilon turbulence model is selected. Moreover, the velocity-pressure condition is fulfilled using the SIMPLE scheme. Worth mentioning that the numerical outcomes have been achieved using a desktop computer equipped with a 3.20 GHz seven-core processor (Intel® Core™ i7-8700 CPU) and 16.0 GB RAM with a time step of 30 s. The residuals for the energy, continuity, momentum, epsilon, and k equations are less than 10^{-6} when the convergence occurred.

3.1. Governing equations

In this numerical simulation, the enthalpy-porosity method [19] is applied to simulate and solve the heat transfer process of columns backfilled with PCM. The conservation equations are presented below:

Continuity equation:

$$\nabla \cdot \left(\rho_{CF}\vec{v}\right) + \frac{\partial \rho_{CF}}{\partial t} = 0 \tag{1}$$

Momentum equation:

$$\nabla \cdot \left(\rho_{PCM} v_i \vec{v}\right) + \frac{\partial \left(\rho_{PCM}\vec{v}\right)}{\partial t} = \rho_{PCM} g_i - \frac{\partial \rho_{PCM}}{\partial x_i} + \nabla \cdot \left(\mu_{PCM} \nabla v_i\right) + S_i \tag{2}$$

$$S_i = C_{mush}\left(v - v_p\right)\frac{(1-\beta)^2}{\left(\beta^3 + \varepsilon\right)} \tag{3}$$

where $\vec{v}$ is the velocity vector, v_i is the velocity component in the i direction, v is the circulation fluid velocity, and v_p is the velocity of the solidified material moving throughout the computational cells during the phase transition. ρ_{CF} and ρ_{PCM} show the densities of circulation fluid and PCM, respectively. S_i is the source term, which shows the relevance of the momentum and porosity in the mushy zone and considers the pressure drop created from the existence of solid material. C_{mush} and ε are known as the constants of mushy zone and computation, respectively [19].

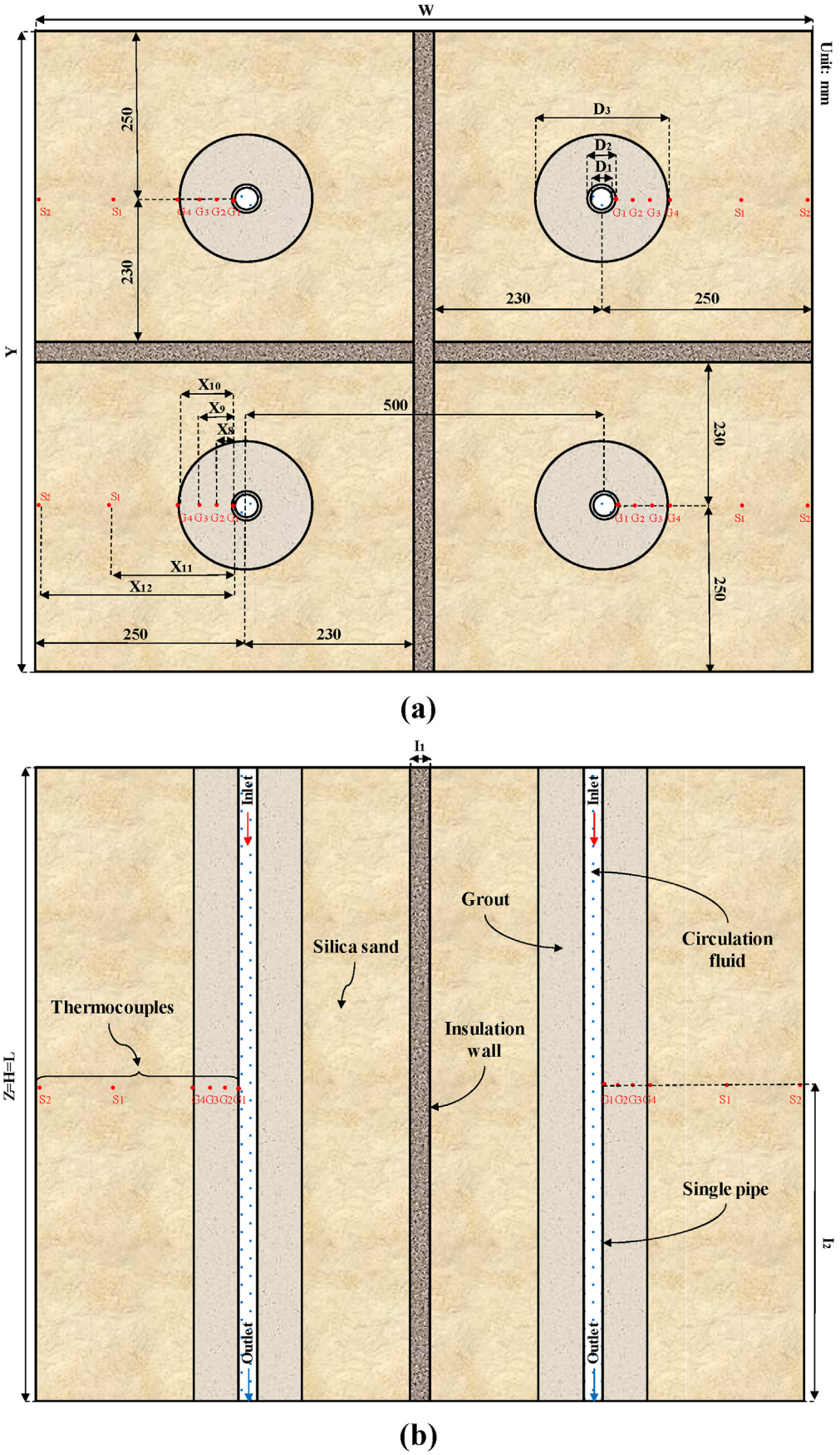

Fig. 6. 2D schematics and the geometrical parameters of the sandbox in the four-column test: (a) Top view, and (b) Front view.

Fig. 7. The four-column test setup: (a) Four separated columns filled with sand and saturated with water, and (b) Connection of the grout columns to the circulation pump.

Energy equation:

$$\nabla \cdot (\rho_{PCM} h_t \mathrm{v}) + \frac{\partial(\rho_{PCM} h_t)}{\partial t} = \nabla \cdot (\lambda_{PCM} \nabla T) + S_e \tag{4}$$

where λ_{PCM} is the thermal conductivity of PCM, S_e is the source term, and h_t is the total enthalpy of PCM calculated by summating latent heat enthalpy (h_{lat}) and sensible heat enthalpy (h_{sens}), as given below:

$$h_t = h_{lat} + h_{sens} \tag{5}$$

$$h_{lat} = \sum_{i=1}^{n} \beta_i L_f \tag{6}$$

$$h_{sens} = h_{ref} + \int_{T_{ref}}^{T} C_p dT \tag{7}$$

where L_f is the latent heat of PCM and β is the liquid fraction that presents the liquefaction level of PCM, which can be expressed as

$$\beta = \begin{cases} 0 & T \le T_{solidus} \\ \dfrac{T - T_{solidus}}{T_{\text{liquidus}} - T_{solidus}} & T_{solidus} < T < T_{\text{liquidus}} \\ 1 & T \ge T_{\text{liquidus}} \end{cases} \tag{8}$$

3.2. Grid independence test

In the numerical approach, two types of grids have been applied to perform the numerical model's meshing, including hexagonal structured and tetrahedral unstructured grids. In the structured meshing, the points of an elemental cell are marked by triple indices (i, j, k) in a 3D simulation, where the central cell is joined by six adjacent cells. Hence, the connectivity is straightforward when using a structured method, leading to easy data management and programming, high-quality solutions, and better convergence with fewer elements than unstructured meshing. Alternatively, in the unstructured meshing, the cells are placed freely inside the computational domain. Consequently, unstructured meshes are efficient for modeling more complex geometries. To evaluate these alternatives, both methods have been used to generate the most suitable grids of the model. The schematic of the meshed model is illustrated in Fig. 8. As can be seen, the volumes near the grout column center have been meshed with finer elements compared to the other volumes, as they are of high importance in the heat transfer process. Moreover, the interfaces between each circulation fluid and pipe, pipe and grout, and grout and sand, were meshed with a four-layer boundary mesh with a transition ratio of 0.15 (see Fig. 8 (a)). The maximum skewness and minimum orthogonal quality values achieved were 0.39 and 0.8, respectively. Table 3 shows the grid independence test conducted for the column containing the reference grout by generating four cases ranging from a coarse mesh to a fine mesh. The created models have been compared in terms of heat exchange rate per meter of grout column depth at the pipe radius after 96 h of operation. By considering the computational speed and accuracy, the third mesh (case 3) is selected for further numerical investigations.

4. Results and discussion

4.1. Single-column test (verification)

The variation of the temperature versus time for the measurement points in the single-column test using experimental and numerical approaches is presented in Fig. 9. The figure shows the temperature response of the grout column and the surrounding sand to the heating of circulating fluid from 20 °C to 40 °C and 50 °C and then cooling down to 20 °C. It can be seen that there is an appropriate agreement between the measured and simulated results, which shows the accuracy and reliability of numerical modeling. As illustrated in Fig. 9, in the temperature variation of G_1 to G_4 during the first 5 h, the temperature difference between G_1 and inlet temperature (approximately 4 °C) can be related to the low heat transfer efficiency between the circulation fluid and the outer surface of the pipe, where the first temperature sensor (G_1) is located. Considering that this temperature loss is not as high as other temperature losses in the figure (in the same period), one can infer to what extent a pipe with higher thermal conductivity can improve the system's thermal behavior. Alternatively, the high-temperature difference between G_1 and G_2 in the first 5 h (approximately 8 °C) and in only 28 mm distance in the grout, compared to the lower differences between G_2-G_3 and G_3-G_4 (approximately 2.5 °C) can be related to the significant influence of the grout-pipe interface. Similar behavior (but with lower

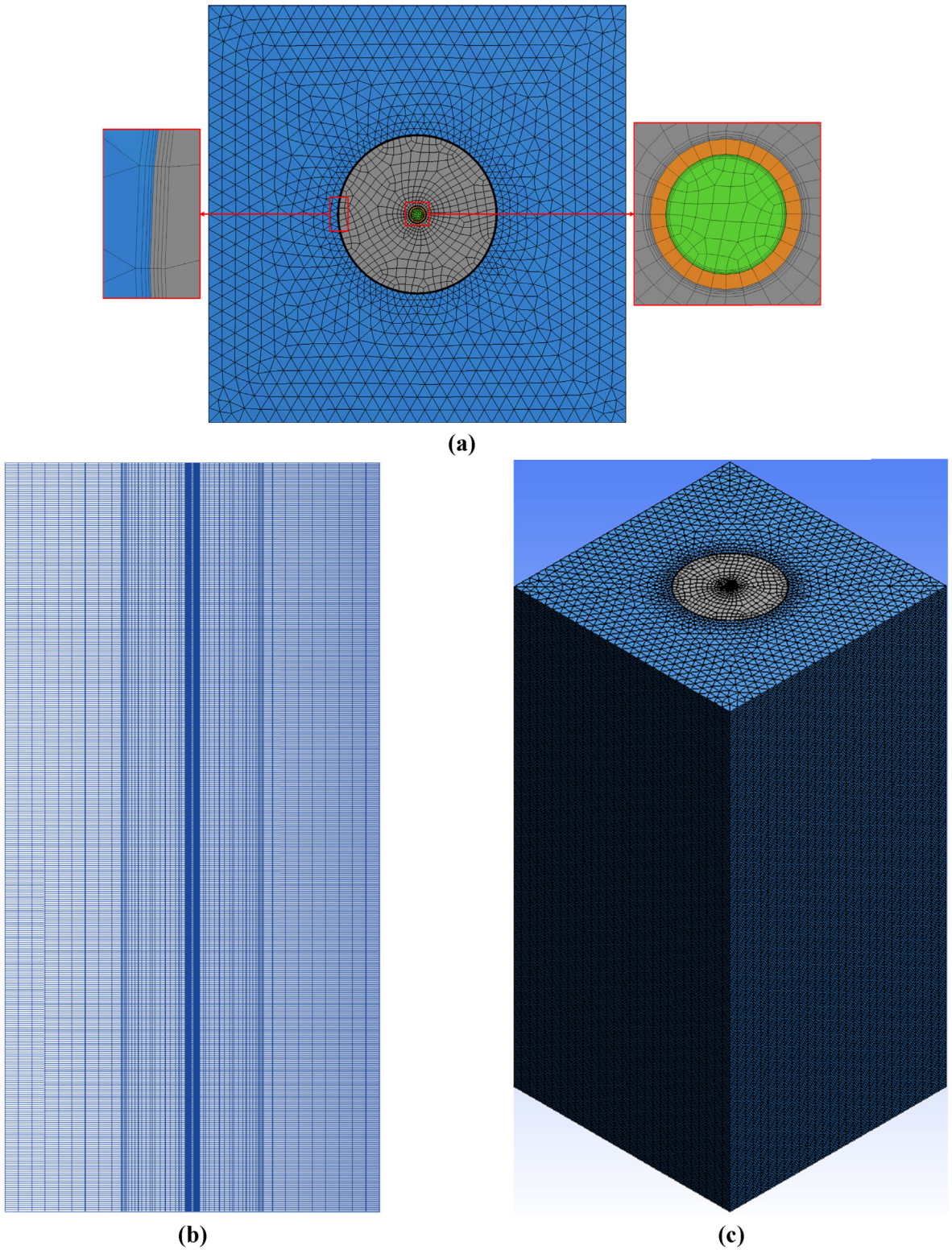

Fig. 8. The meshing of the model: (a) Top view, (b) Front view, and (c) 3D view.

Table 3
Grid independence test.

	Case 1	Case 2	Case 3	Case 4
Elements' total number	428,437	795,169	1,129,328	1,564,718
Heat exchange rate per meter of grout column depth at the pipe radius after 96 h of operating [W/m]	212.72	213.39	213.84	213.81

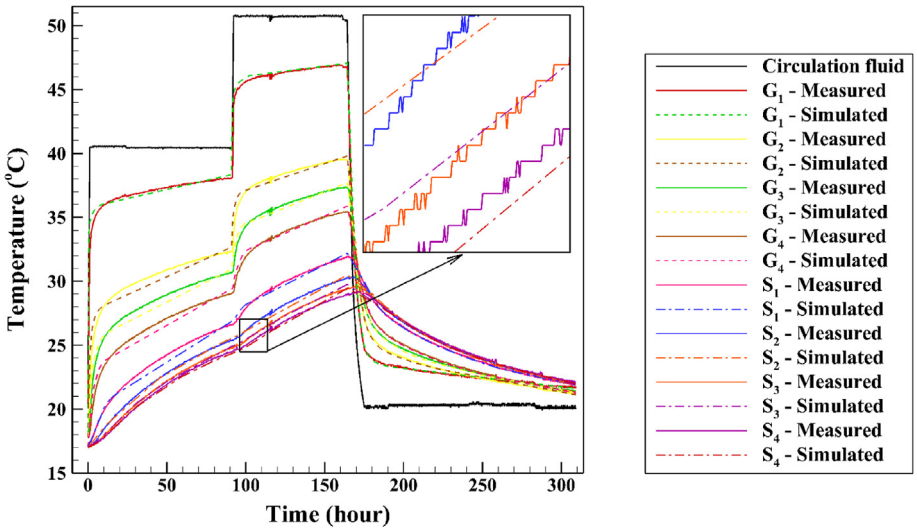

Fig. 9. Variation of the temperature versus time for the measurement points in the single-column test using experimental and numerical approaches.

intensity) can be seen at the grout-sand interface, highlighting the importance of interfaces, especially the grout-pipe interface, on the system's overall thermal behavior.

4.2. Four-column test (comparison)

One complete cycle of heating and cooling with temperature variations from 20 °C to 50 °C and then back to 20 °C have been applied to the circulating fluid during the test. The four grout columns used in the setup include a reference grout (commercial grout) and three newly enhanced grouts with high thermal conductivity (using graphite-based materials) and high TES capacity (using MPCM and SSPCM). The idea is to ensure as similar test conditions as possible for the four grout columns to allow a proper comparison between their thermal behavior to show the newly developed grouts' efficiency.

Fig. 10 illustrates the time - dependent temperature field distribution in the four-column test during one complete cycle. The column containing enhanced grout reaches the temperature levels faster than the other grout columns in the heating operation, thanks to its high thermal conductivity. This time difference between the enhanced grout and the others is quite significant at the temperature level of 45 °C almost after 60 h of heat injection. Similarly, in the cooling operation, when decreasing the circulation fluid temperature from 50 °C to 20 °C, thermally enhanced grout cooled down earlier than the other grouting materials. In contrast, the mixture of enhanced grout and MPCM reached the temperature levels later than the others, specifically at the temperature level of

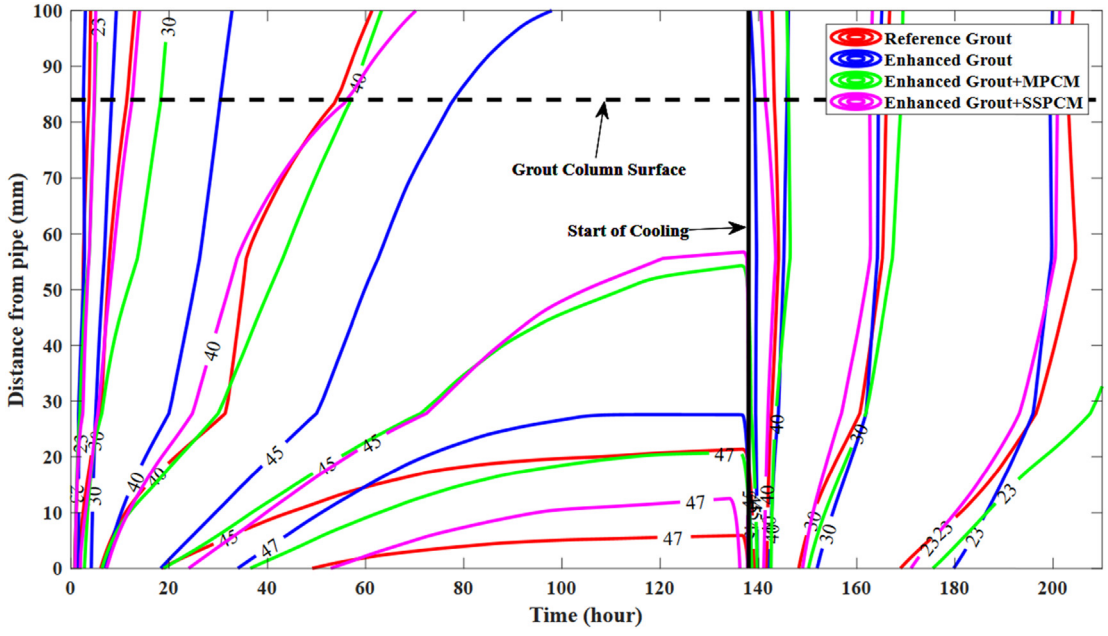

Fig. 10. Temperature field distribution in the four-column test at different operation hours during one complete cycle.

around 30 °C, near the range of phase transition temperature of MPCM. This effect can be explained by the presence of MPCM in the enhanced grout mixture and the corresponding increase in its heat capacity. However, after the complete melting of the MPCM particles, which occurs around 20 h after the start of heat injection, the mixture cannot store more thermal energy, and accordingly, it dissipates the heat to the surroundings. In cooling operation, like in heating mode, it takes longer for the mixture of MPCM and enhanced grout to reach lower temperature levels compared to the rest of grout materials, especially at the temperature level of 23 °C. The reason that no such behavior is observed in the grout column with SSPCM can be related to the broader range of phase transition temperatures of the SSPCM compared to the MPCM.

Fig. 11 shows the comparison of the thermocouples' thermal responses during the full duration of heat injection between the different grout columns. Each plot corresponds to a given sensor location. In the first measurement point (G_1), which is located on the PE pipe's surface, no significant difference is observed between the temperatures registered during the 30 h in the four grout columns. However, sensor located farther away (i.e., at G_2, G_3, and G_4), show increasingly larger temperature differences. At the same measurement points (G_2, G_3, and G_4), the highest temperature registered is usually in the grout column with high thermal conductivity (enhanced grout), whereas the lowest temperature is in the one with MPCM. This issue is once again related to the heat absorption of the PCM particles during the phase change (solid to liquid) that hindered the temperature increase. However, after approximately 17 h, when the temperature at G_4 increased to 28.8 °C (the peak transition temperature of MPCM), all the MPCM particles incorporated in the grout column are already subjected to phase transition. Accordingly, there is no further hindrance against the increase in temperature, and thus the temperature gradient registered at G_4 increases afterward. Similar behavior is observed in the grout column with SSPCM after approximately 6 h when the temperature at G_4 reached 24 °C (to the peak transition temperature of SSPCM). This matter suggests that most of the SSPCM incorporated in the grout column are subjected to the phase change (solid to liquid) at nearly 24 °C. Following that, the temperature gradient registered at G_4 is considerably increased. The intersection points of the horizontal line (chosen as 24 °C and 28.8 °C, i.e., the melting points of SSPCM and MPCM, respectively) and the graphs of the temperature variation registered at each measurement point

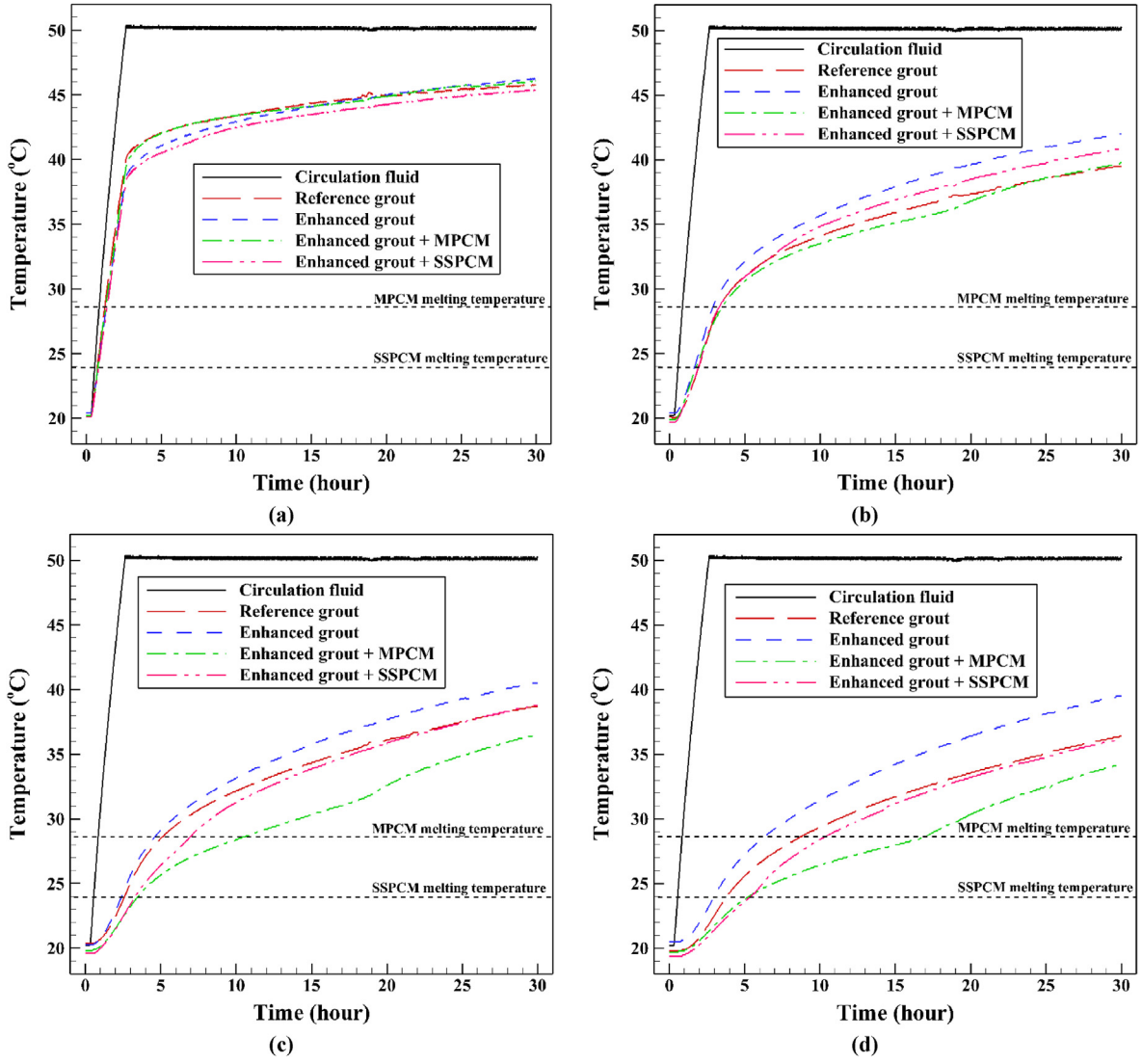

Fig. 11. Comparison of the thermocouples' thermal responses during the 30 h of the heat injection from 20 °C to 50 °C to different grout columns: (a) G_1, (b) G_2, (c) G_3, and (d) G_4.

in different grout columns indicate the time difference needed to reach the same temperature at a certain distance from the circulating pipe when various grouting materials are applied. As shown in the same figure, the longer the distance from the pipe in the grout column, the longer the time needed to reach the same temperature in different grout columns. At G_4, the time difference to reach 28.8 °C between the grout column with enhanced grout and the grout with MPCM is more than 10 h. This issue can be related to the faster heat transfer in the grout column with enhanced grout compared to the combined delays caused by the phase change and the lower thermal conductivity of the MPCM. Fig. 12 shows the time needed for various thermocouples in different grout columns to reach the same temperatures of 21 °C, 28.3 °C, 35 °C, and 40 °C during the heating process. In all cases, the shortest time for reaching the desired temperature was seen in the column with enhanced grout and the longest time in the grout column containing MPCM with enhanced grout. This issue supports the observations previously presented in Fig. 11.

Worth mentioning that these time differences created in four grout columns can bring advantages or disadvantages to the GSHP system, depending on the system's goal. Thermally enhanced grout in a BHE will benefit the GSHP performance aimed at conventional heating and cooling by increasing the heat transfer at the shortest time to or from the surrounding ground during heat dissipation or

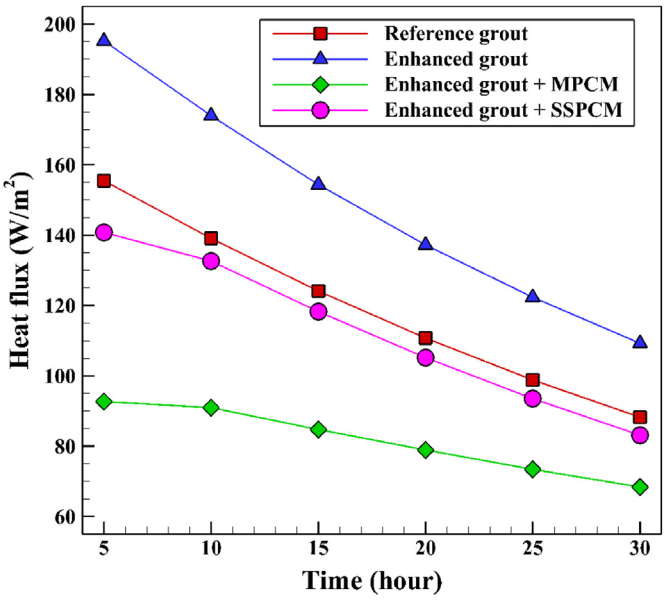

Fig. 13. Heat flux per unit of surface area at the borehole radius for different grout columns during the 30 h of the heating operation from 20 °C to 50 °C.

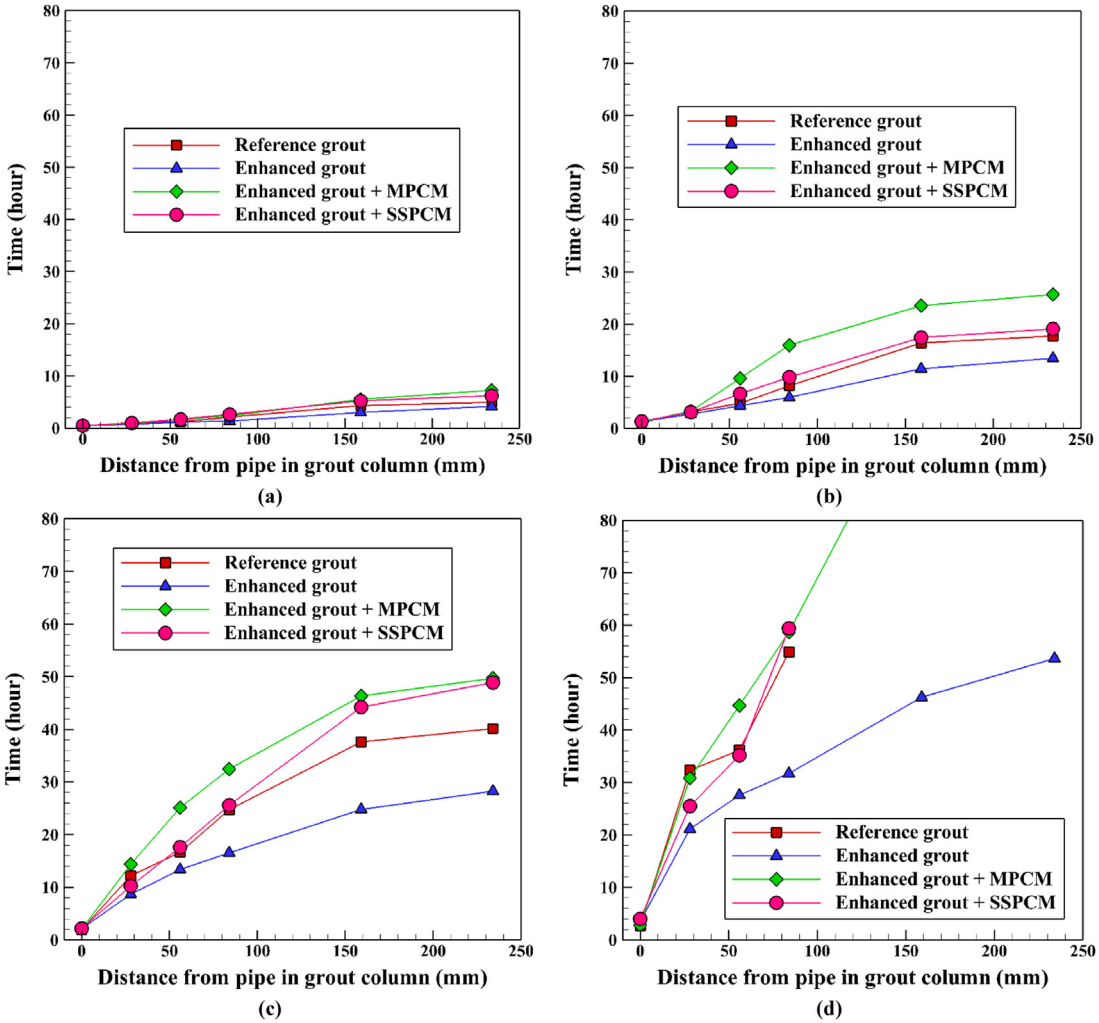

Fig. 12. Time needed for various thermocouples in different grout columns to reach the same temperatures during the heat injection: (a) 21 °C, (b) 28.3 °C, (c) 35 °C, and (d) 40 °C.

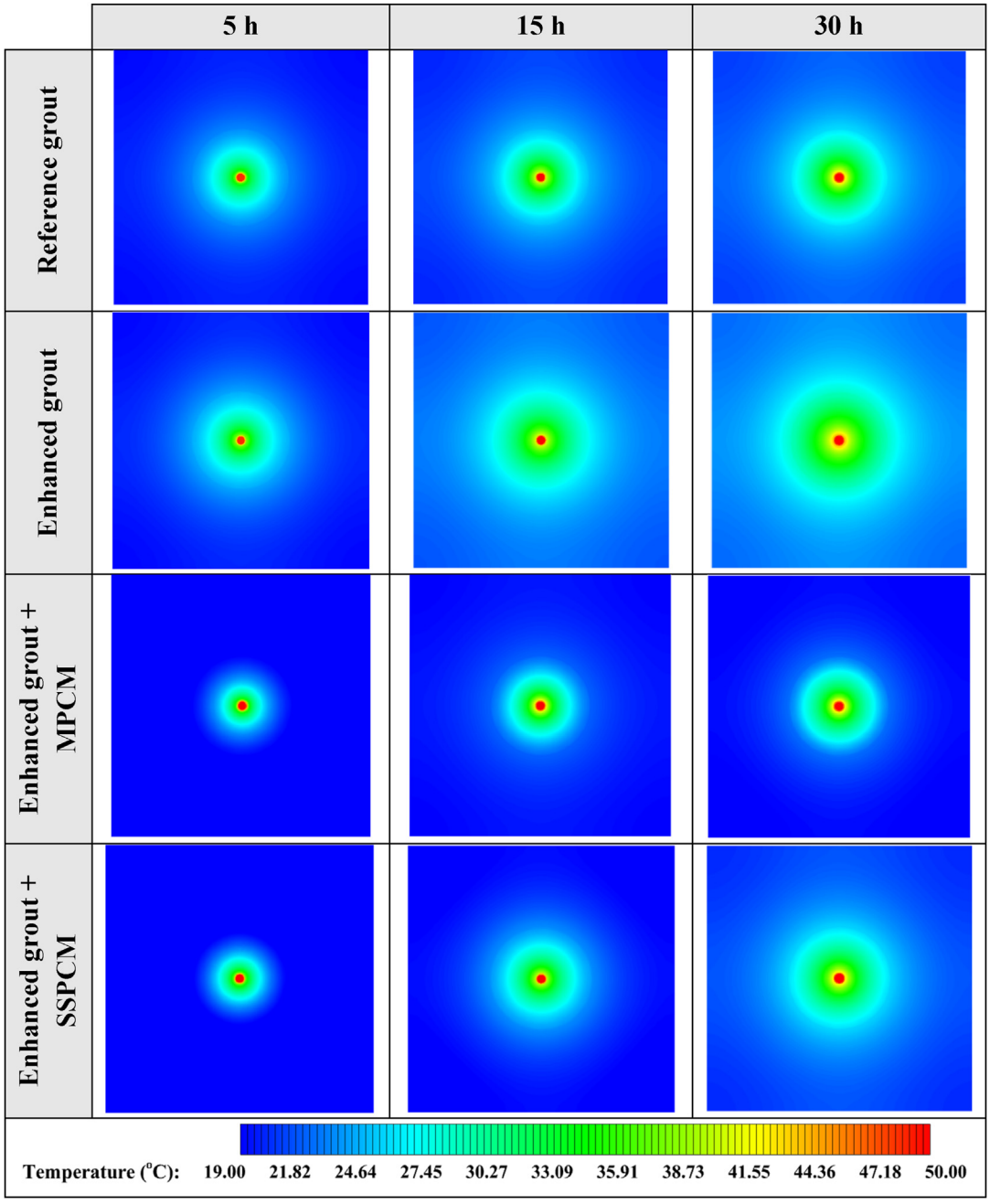

Fig. 14. 2D contours of the temperature distribution of the sandbox in the four-column test during the heating operation at different operation hours (Top view at Z = 0).

extraction, respectively. However, the use of enhanced grout will not be a good idea when the system is targeted at storing energy. Here is when the MPCM grout can play a vital role in the BTES system because of its higher heat capacity and lower thermal conductivity than reference and thermally enhanced grouts. Therefore, the MPCM particles will not be suitable for typical heating and cooling operation, as they are practical for storing the thermal energy and reusing it daily or seasonally, not thermal exchanging with the surroundings.

Fig. 13 illustrates the total surface heat flux at the borehole radius (here the lateral surface of the grout column) for different grout columns during the 30 h of the heat injection from 20 °C to 50 °C. At the beginning of the heat exchange process, the temperature difference between the system and the circulation fluid is at its maximum level, which resulted in achieving the highest values of heat flux for each grout column. Subsequently, the thermal energy transfer from the circulation fluid to the grout and sand decreases because of the reduced temperature differences between the grout and the heat carrier fluid. The presence of MPCM particles inside the enhanced grout decreases the diagram slope notably, keeping the value of heat flux per unit of grout column surface transferred to the sand more constant. On the contrary, the thermally enhanced grout significantly improves the heat dissipation rate from the working fluid to the sand. As can be seen from Fig. 13, the maximum and minimum heat fluxes are achieved by the grout column containing enhanced grout and the grout column

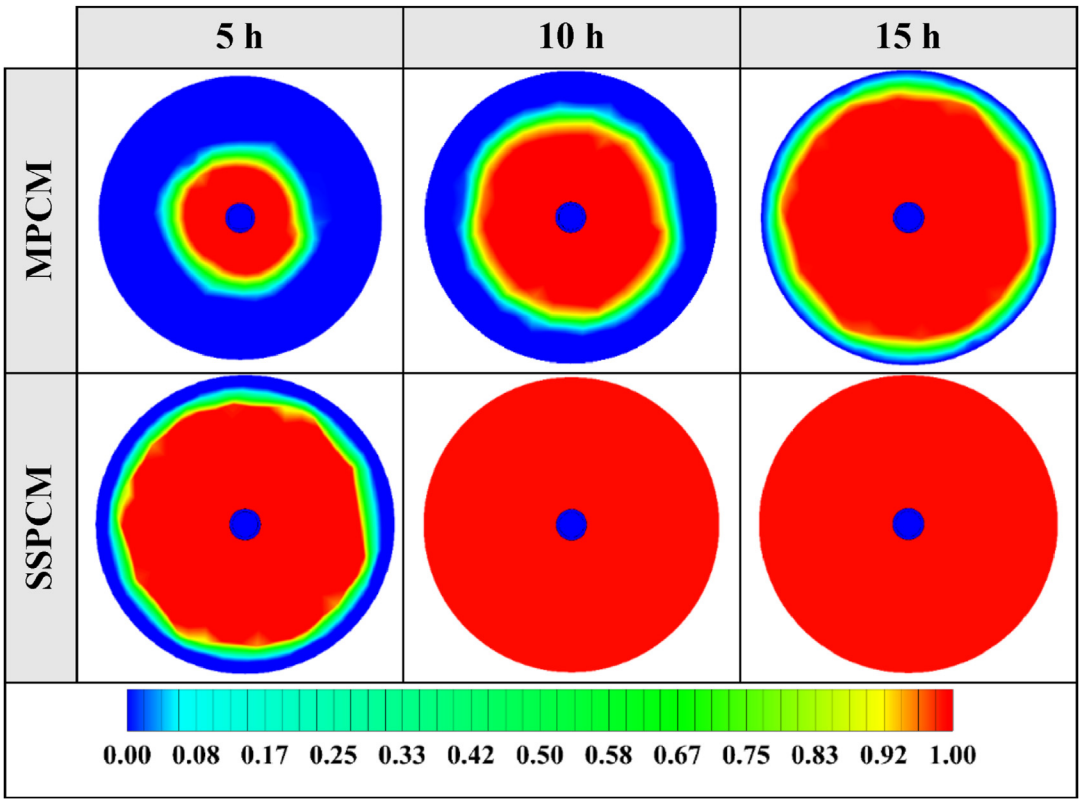

Fig. 15. 2D contours of the liquid fraction of the grout columns containing MPCM and SSPCM in the four-column test during the heating operation at different operation hours (Top view at Z = 0).

backfilled with the mixture of enhanced grout and MPCM, respectively. 2D contours of the temperature distribution of the sandbox in the four-column test during the heating process at different operating hours are presented in Fig. 14 (see also Fig. A1 (Appendix)). The thermal radius around the pipe increases over time in all grout columns. Heat transfer has occurred mainly in the column containing enhanced grout, which shows its significant capability of heat dissipation to be used as a backfill/grout material in a BHE. In contrast, the minimum heat exchange between each working fluid and the surroundings corresponds to the column filled with a mixture of enhanced grout and MPCM (see also Fig. 11), related to the gradual melting of the MPCM. Hence, heat storage capacity of MPCM enables it to absorb the heat from heat carrier fluid circulating inside the pipe, illustrating the notable capability of the mixture of MPCM and enhanced grout to be applied in a BTES system. Similarly, in the other column filled with a mixture of enhanced grout and SSPCM, the same trend can be observed, but with a higher rate of heat transfer from the grout column to the sand. This difference in the heat transfer can be related to the higher thermal conductivity and lower peak melting temperature of this mixture compared with the MPCM mixture (see Table 1). Hence, the grout column containing the enhanced grout and SSPCM is subjected to a higher rate of heat transfer, which has caused SSPCM to be melted entirely about 6 h from the start of heat injection (see Figs. 11 and 15). Once the SSPCM reaches its maximum TES capacity, continuing heat injection to the grout column increases the sand temperature clearly above the level that is reached in the grout column filled with MPCM. 3D contours of the temperature distribution of the sandbox in the four-column test can be found in Fig. A2 (Appendix). 2D contours of the liquid fraction of the grout columns containing MPCM and SSPCM in the four-column test during the heating operation at different operation hours are illustrated in Fig. 15. According to this figure and Fig. 11, it can be concluded that MPCM is melted completely around 17 h after the start of the heat injection. This issue can be justified by MPCM's higher peak melting temperature than SSPCM's, which resulted in increasing the time needed for MPCM to use its maximum capacity in storing thermal energy. Thus, the time difference of a complete melting of the MPCM and SSPCM is approximately 11 h.

5. Conclusions

In this study, different advanced grouting materials, such as enhanced grout, a mixture of enhanced grout and micro-encapsulated phase change material (MPCM), and a mixture of enhanced grout and shape stabilized phase change material (SSPCM), have been experimentally evaluated using a laboratory-scale prototype in combination with 3D numerical simulation. Based on the literature reviewed, there have been just a few numerical studies on implementing phase change materials in the borehole heat exchangers, and the thermal energy storage application of the borehole heat exchangers has not yet been evaluated in detail. The objective is to study the improvement in the thermal conductivity and thermal energy storage capacity of the three novel grouting formulations compared to a reference grout and investigate the potential of the developed grouts to be applied in a borehole heat exchanger and borehole thermal energy storage systems.

Verifying the numerical results with the experimental data showed good agreement indicating the reliability of the numerical simulations. The experimental and numerical outcomes showed that the grout column with enhanced grout reached the highest total surface heat flux at the borehole radius. In contrast, the grout column backfilled with the mixture of enhanced grout and

microencapsulated phase change material achieved the lowest heat flux (almost 37% lower than enhanced grout), thanks to the incorporation of microencapsulated phase change material into the mixture. Despite the faster melting process of SSPCM during the beginning hours of heat injection compared to MPCM, the mushy zone thickness created in the SSPCM mixture (mutual existence of solid and liquid phases) is relatively smaller than that in the MPCM mixture, which may be related to the lower thermal conductivity, specific heat capacity and latent heat of MPCM.

In other words, the grout column with the increased thermal conductivity revealed its heat transfer effectiveness by the quickest reaction toward temperature differences compared with the other three grout columns with reference and phase change materials. Accordingly, when a GSHP system is equipped with a borehole heat exchanger backfilled with the thermally enhanced grout, the heat injection to and extraction from the ground during summer and winter will improve enormously, strengthening the whole system's performance. Moreover, when the borehole heat exchanger contains phase change materials, specifically MPCM, the objective of the GSHP system will be different from a typical shallow geothermal system. Based on the high thermal energy storage capacity of the MPCM, the system performance can be boosted daily or seasonally. In the daily mode, the MPCM stores the thermal energy during the day to minimize the peak load and then reuses the energy during the night. In seasonal operation, the heat is absorbed in the MPCM during summer, and then it can be recovered by the MPCM solidification process for winter. In both operation modes, the GSHP system performance will be improved owing to the enriched capability of MPCM in energy storage.

In conclusion, thermally enhanced grout indicated a significant increase in thermal conductivity compared with that in the reference grout column, demonstrating its ability to provide higher rates of heat transfer, which are beneficial for borehole heat exchangers. Moreover, it is concluded that adding a microencapsulated phase change material to the thermally enhanced grout improves the heat storage capacity remarkably, providing high potential for storing thermal energy for the final mixture. The mixture of enhanced grout and shape stabilized phase change material is found to be inferior to the microencapsulated phase change material solution due to the lower melting temperature and increased thermal conductivity of the mixture.

This research opens further investigation opportunities to optimize the mixture properties for a given application or scenario. Besides, the developed materials evaluated in the present paper will be applied in a real borehole thermal energy storage system to study their capability in storing heat. In future experiments, the integration of more sensitization elements will also be taken into account.

Declaration of competing interest

The authors declare that they have no known competing financial interests or personal relationships that could have appeared to influence the work reported in this paper.

Acknowledgments

This article is part of a project that has received funding from the European Union's Horizon 2020 research and innovation programme under grant agreement No 727583.

Funding for open access charge: AYUDAS A INVESTIGADORES PREDOCTORALES PARA LA PUBLICACIÓN DE ARTÍCULOS DE INVESTIGACIÓN EN ABIERTO (PAID-12-21) by Universitat Politècnica de València.

Appendix

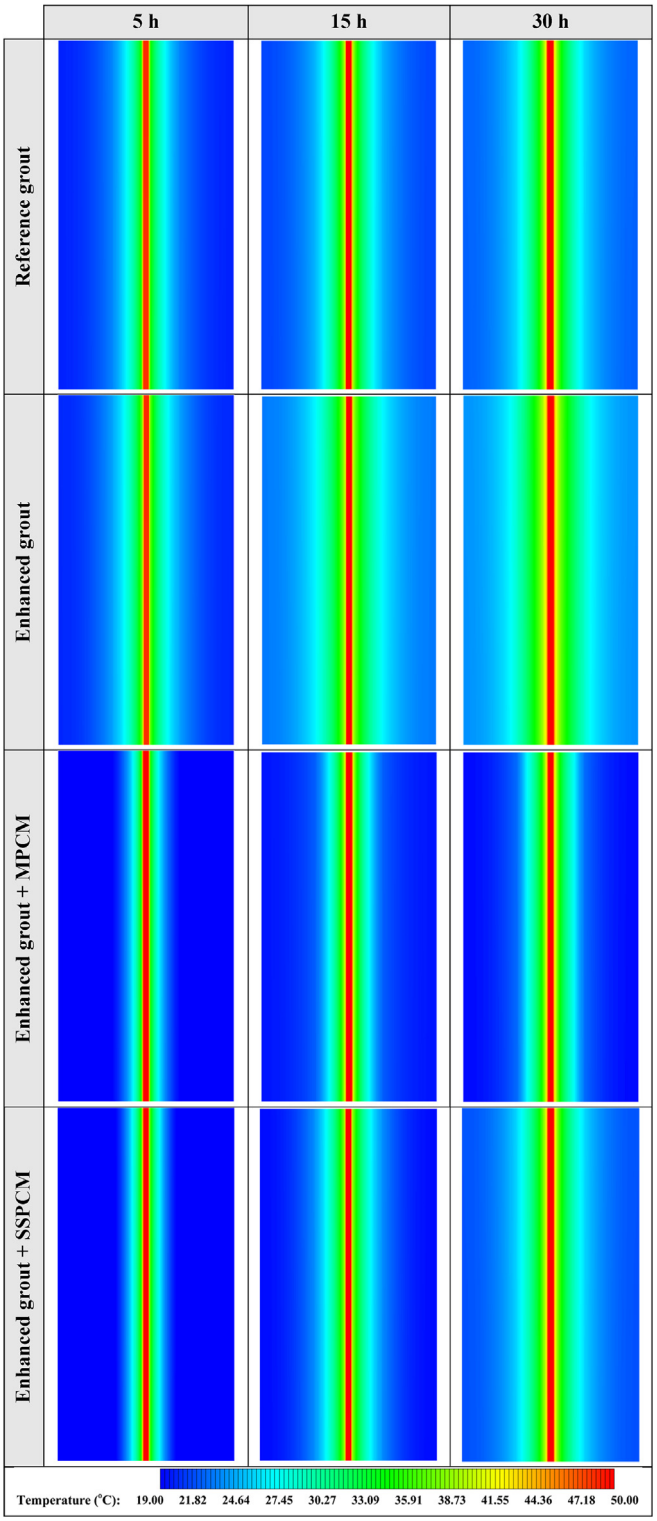

Fig. A1. 2D contours of the temperature distribution of the sandbox in the four-column test during the heating operation at different operation hours (Front view, middle plane).

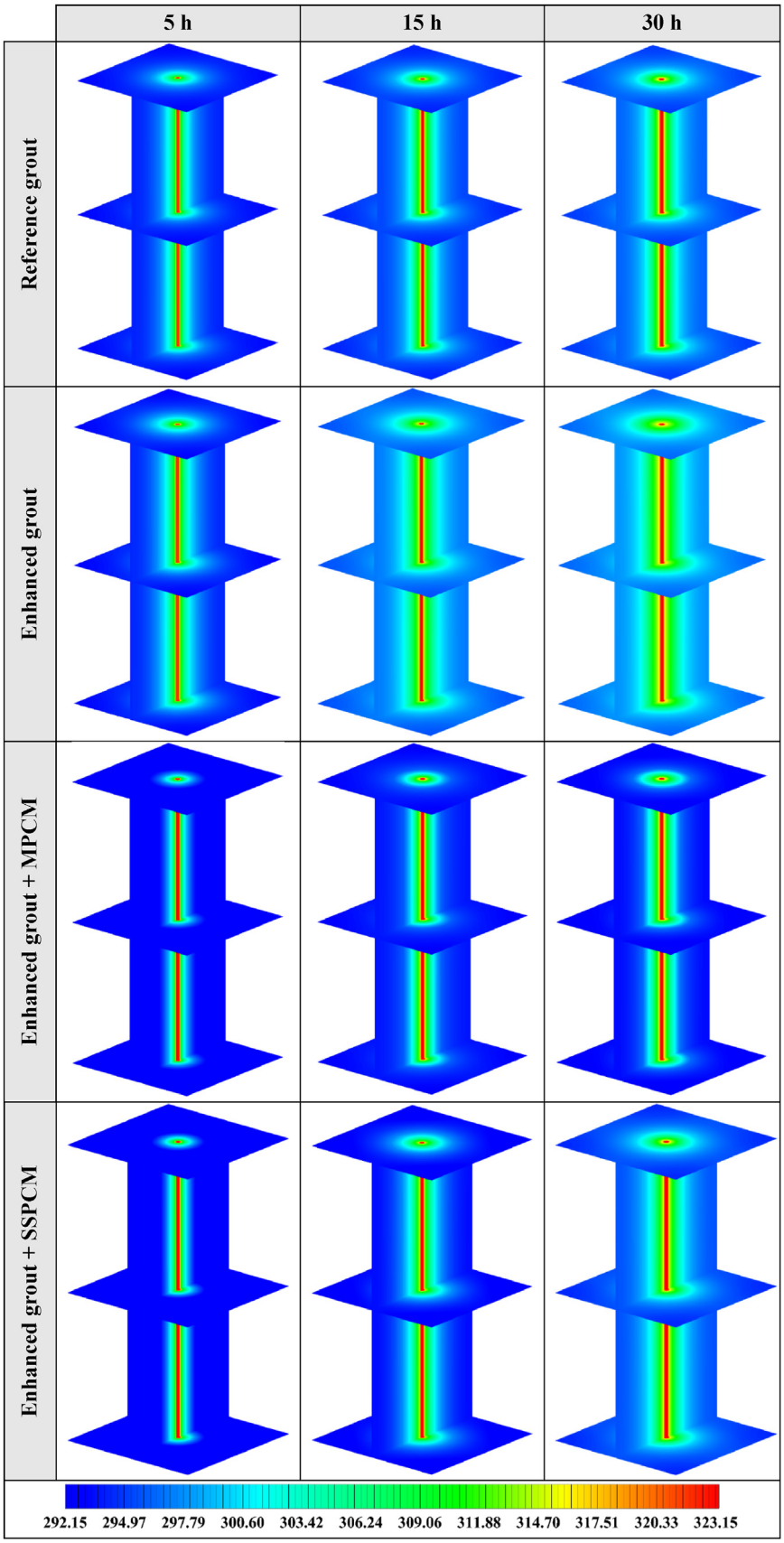

Fig. A2. 3D contours of the temperature distribution of the sandbox in the four-column test during the heat injection at different operation hours.

References

[1] Adela Ramos-Escudero, M. Socorro García-Cascales, Jose M. Cuevas, Burkhard Sanner, Javier F. Urchueguía, Spatial analysis of indicators affecting the exploitation of shallow geothermal energy at European scale, Renew. Energy 167 (2021) 266–281.

[2] K.P. Tsagarakis, L. Efthymiou, A. Michopoulos, A. Mavragani, A.S. Anđelković, F. Antolini, M. Bacic, D. Bajare, M. Baralis, W. Bogusz, S. Burlon, J. Figueira, M.S. Genç, S. Javed, A. Jurelionis, K. Koca, G. Ryżyński, J.F. Urchueguía, B. Žlender, A review of the legal framework in shallow geothermal energy in selected European countries: need for guidelines, Renew. Energy 147 (2020) 2556–2571.

[3] Hossein Javadi, Seyed Soheil Mousavi Ajarostaghi, Marc A. Rosen, Mohsen Pourfallah, A comprehensive review of backfill materials and their effects on ground heat exchanger performance, Sustainability 10 (2018) 4486.

[4] Hossein Javadi, Seyed Soheil Mousavi Ajarostaghi, Marc A. Rosen, Mohsen Pourfallah, Performance of ground heat exchangers: a comprehensive review of recent advances, Energy 178 (2019) 207–233.

[5] B. Badenes, M.A.M. Sanner, J.M. Pla, F. Cuevas, F. Bartoli, R.M. Ciardelli, A.N. González, P. Ghafar, L.L. Fontana, J.F. Zuñiga, Urchueguía, Development of advanced materials guided by numerical simulations to improve performance and cost-efficiency of borehole heat exchangers (BHEs), Energy 201 (2020), 117628.

[6] S. Gehlin, Borehole thermal energy storage, in: Advances in Ground-Source Heat Pump Systems, Woodhead Publishing, Elsevier, 2016, pp. 295–327.

[7] M. Reuss, The use of borehole thermal energy storage (BTES) systems, in: Advances in Thermal Energy Storage Systems, Woodhead Publishing, Elsevier, 2015, pp. 117–147.

[8] Jin Long Wang, Jing De Zhao, Ni Liu, Numerical simulation of borehole heat transfer with phase change material as grout, Appl. Mech. Mater. 577 (2014) 44–47.

[9] Di Qi, Liang Pu, Futao Sun, Yanzhong Li, Numerical investigation on thermal performance of ground heat exchangers using phase change materials as grout for ground source heat pump system, Appl. Therm. Eng. 106 (2016) 1023–1032.

[10] Yi Lyne, Halime Paksoy, Mohammed Farid, Laboratory investigation on the use of thermally enhanced phase change material to improve the performance of borehole heat exchangers for ground source heat pumps, Int. J. Energy Res. 43 (2019) 4148–4156.

[11] Douglas D. Cortes, Nasirian Ali, Dai Sheng, Smart ground-source borehole heat exchanger backfills: a numerical study, in: International Symposium on Energy Geotechnics, Springer, 2018, pp. 27–34.

[12] Ahmad Aljabr, Andrew Chiasson, Alhajjaji Amr, Numerical modeling of the effects of micro-encapsulated phase change materials intermixed with grout in vertical borehole heat exchangers, Geothermics 96 (2021), 102197.

[13] Fei Chen, Jinfeng Mao, Shangyuan Chen, Chaofeng Li, Pumin Hou, Lu Liao, Efficiency analysis of utilizing phase change materials as grout for a vertical U-tube heat exchanger coupled ground source heat pump system, Appl. Therm. Eng. 130 (2018) 698–709.

[14] Fei Chen, Jinfeng Mao, Chaofeng Li, Pumin Hou, Yong Li, Zheli Xing, Shangyuan Chen, Restoration performance and operation characteristics of a vertical U-tube ground source heat pump system with phase change grouts under different running modes, Appl. Therm. Eng. 141 (2018) 467–482.

[15] Weibo Yang, Rui Xu, Binbin Yang, Jingjing Yang, Experimental and numerical investigations on the thermal performance of a borehole ground heat exchanger with PCM backfill, Energy 174 (2019) 216–235.

[16] H.Y. Lei, C.S. Dai, Heat transfer analysis of centric borehole heat exchanger with different backfill materials, in: Proceedings of the World Geothermal Congress, Melbourne, Australia, 2015, pp. 19–25.

[17] Xiangli Li, Cang Tong, Duanmu Lin, Liangkan Liu, Research on U-tube heat exchanger with shape-stabilized phase change backfill material, Procedia Eng. 146 (2016) 640–647.

[18] Xiangli Li, Cang Tong, Duanmu Lin, Liangkan Liu, Study of a U-tube heat exchanger using a shape-stabilized phase change backfill material, Sci. Technol. Built Environ. 23 (2017) 430–440.

[19] Hossein Javadi, Javier F. Urchueguia, Seyed Soheil Mousavi Ajarostaghi, Borja Badenes, Numerical study on the thermal performance of a single U-tube borehole heat exchanger using nano-enhanced phase change materials, Energies 13 (2020) 5156.

[20] Michele Bottarelli, Aleksandar Georgiev, Ahmet Alper Aydin, Yuehong Su, Charles Yousif, Ground-source Heat Pumps Using Phase Change Materials, European Geothermal Congress, Pisa, Italy, 2013, 3-7 June.

[21] Michele Bottarelli, Marco Bortoloni, Yuehong Su, Charles Yousif, Ahmet Alper Aydın, Aleksandar Georgiev, Numerical analysis of a novel ground heat exchanger coupled with phase change materials, Appl. Therm. Eng. 88 (2015) 369–375.

[22] Michele Bottarelli, Marco Bortoloni, Yuehong Su, Heat transfer analysis of underground thermal energy storage in shallow trenches filled with encapsulated phase change materials, Appl. Therm. Eng. 90 (2015) 1044–1051.

[23] Mingkan Zhang, Xiaobing Liu, Kaushik Biswas, Joseph Warner, A three-dimensional numerical investigation of a novel shallow bore ground heat exchanger integrated with phase change material, Appl. Therm. Eng. 162 (2019), 114297.

[24] Joseph Warner, Xiaobing Liu, Liang Shi, Ming Qu, Mingkan Zhang, A novel shallow bore ground heat exchanger for ground source heat pump applications—model development and validation, Appl. Therm. Eng. 164 (2020), 114460.

[25] Joseph Keith Warner, Feasibility Study of a Novel Ground Heat Exchanger Using Phase-Change Materials, A Thesis Presented for the Master of Science Degree, University of Tennessee, Knoxville, 2019.

[26] Di Qin, Zhengxuan Liu, Yuekuan Zhou, Zhongjun Yan, Dachuan Chen, Guoqiang Zhang, Dynamic performance of a novel air-soil heat exchanger coupling with diversified energy storage components—modelling development, experimental verification, parametrical design and robust operation, Renew. Energy 167 (2021) 542–557.

[27] Zhengxuan Liu, Pengchen Sun, Mingjing Xie, Yuekuan Zhou, Yingdong He, Guoqiang Zhang, Dachuan Chen, Shuisheng Li, Zhongjun Yan, Di Qin, Multivariant optimization and sensitivity analysis of an experimental vertical earth-to-air heat exchanger system integrating phase change material with Taguchi method, Renew. Energy 173 (2021) 401–414.

[28] Ammar Hassanpour, Mehdi Borji, Behrooz M. Ziapour, Admin Kazemi, Performance analysis of a cascade PCM heat exchanger and two-phase closed thermosiphon: a case study of geothermal district heating system, Sustain. Energy Technol. Assessments 40 (2020), 100755.

[29] Y. Rabin, E. Korin, Incorporation of phase-change materials into a ground thermal energy storage system: theoretical study, Energy Res. Technol. 118 (1996) 237–241.

[30] R. Hirmiz, H.M. Teamah, M.F. Lightstone, J.S. Cotton, Performance of heat pump integrated phase change material thermal storage for electric load shifting in building demand side management, Energy Build. 190 (2019) 103–118.

[31] Hüseyin Benli, Aydın Durmuş, Evaluation of ground-source heat pump combined latent heat storage system performance in greenhouse heating, Energy Build. 41 (2009) 220–228.

[32] Hüseyin Benli, Energetic performance analysis of a ground-source heat pump system with latent heat storage for a greenhouse heating, Energy Convers. Manag. 52 (2011) 581–589.

[33] Wanfang Zhao, Zhongting Hu, Wei He, Sheng Zhang, Hancheng Yu, Gaofei Xu, Hongbing Chen, Intermittent mode analysis of a borehole ground heat exchanger with novel phase change backfill materials, Appl. Therm. Eng. 189 (2021), 116716.

[34] N. Zhu, P. Hu, Y. Lei, Z. Jiang, F. Lei, Numerical study on ground source heat pump integrated with phase change material cooling storage system in office building, Appl. Therm. Eng. 87 (2015) 615–623.

[35] Parham Eslami-nejad, Michel Bernier, A preliminary assessment on the use of phase change materials around geothermal boreholes, Build. Eng. 119 (2013) 312.

[36] M.M. Mousa, A.M. Bayomy, M.Z. Saghir, Phase change materials effect on the thermal radius and energy storage capacity of energy piles: experimental and numerical study, Int. J. Thermofluids 10 (2021), 100094.

[37] Weibo Yang, Binbin Yang, Feng Wang, Naidong Jing, Numerical Evaluations on the Effects of Thermal Properties on the Thermo-Mechanical Behaviour of a Phase Change Concrete Energy Pile, Energy and Built Environment, 2021.

[38] R. Elhashmi Alkhwildi, A. Chiasson, Parametric modeling and simulation of Low temperature energy storage for cold-climate multi-family residences using a geothermal heat pump system with integrated phase change material storage tank, Geothermics 86 (2020), 101864.

[39] Liang Pu, Lingling Xu, Shengqi Zhang, Yanzhong Li, Optimization of ground heat exchanger using microencapsulated phase change material slurry based on tree-shaped structure, Appl. Energy 240 (2019) 860–869.

[40] P. McKenna, W.J.N. Turner, D.P. Finn, Thermal energy storage using phase change material: analysis of partial tank charging and discharging on system performance in a building cooling application, Appl. Therm. Eng. 198 (2021), 117437.

[41] Jun-Seo Jeon, Seung Rae Lee, Min Jun Kim, Benefit of phase change material on the performance of horizontal ground heat exchanger: a numerical study, in: World Congress on Advances in Civil, Environmental, and Materials Research, Jeju Island, 2016.

[42] Pejman Keikhaei Dehdezi, Matthew R. Hall, Andrew R. Dawson, Enhancement of soil thermo-physical properties using microencapsulated phase change materials for ground source heat pump applications, Appl. Mech. Mater. 110 (2012) 1191–1198.

[43] Silvia Barbi, Francesco Barbieri, Simona Marinelli, Bianca Rimini, Sebastiano Merchiori, Barbara Larwa, Michele Bottarelli, Monia Montorsi, Phase change material-sand mixtures for distributed latent heat thermal energy storage: interaction and performance analysis, Renew. Energy 169 (2021) 1066–1076.

[44] Selçuk Erol, François Bertrand, Efficiency of various grouting materials for borehole heat exchangers, Appl. Therm. Eng. 70 (2014) 788–799.

[45] Liang Pu, Di Qi, Li Kang, Hongbo Tan, Yanzhong Li, Simulation study on the thermal performance of vertical U-tube heat exchangers for ground source heat pump system, Appl. Therm. Eng. 79 (2015) 202–213.